TÉCNICO LISBOA

Numerical Modeling of Earth Dam Breaching by Overtopping

André F. P. Lopes

Under the supervision of Professor Rui M. L. Ferreira and Professor Maria Rafaela Pinheiro Cardoso

November 2015

1 Abstract

An existing numerical model STAV2D is adapted to a new language with the purpose of producing a toolbox for MATLAB called STAVBreach, specialized in the simulation of breaching of embankment dams. Both the language and software used will provide a more practical user interface for future work and learning.

The model is validated for several well know problems with analytical solutions that represent particular cases of the shallow water equations in both 1D and 2D environments with and without sediment transport.

Experimental work performed at LNEC was conducted to model the dam breaching process in small scale dams with good geotechnical design requirements. The results obtained provided both direct and indirect estimations of the breach hydrographs as well as a documented breaching process.

Finally numerical simulations are made for similar conditions as the experiments and the results are compared in order to validate the numerical model.

This work has demonstrated the need to consider mass displacement in the breaching process of dams in dam breach simulations, as the instantaneous enlargement of the breach and sediment concentration increase, disrupting the flow. And that the geotechnical instabilization engine developed is able to simulate the mass displacement phenomena.

2 Introduction

Water reservoirs are fundamental to socio-economic development since the beginning of human history. They mainly provide water and energy but many other secondary uses can be described from providing food (aquaculture) to touristic activities. Although reservoirs can be natural, increased demographic pressure has forced making to build dams to store water, therefore inducing flood hazards on downstream valleys. Dam failures lead to extreme economical losses, environmental damages and are likely to cause human casualties. They may fail due to various causes, being overtopping the most common in earth dams (ICOLD (2013)).

The most recent advances in modeling the breaching process of embankment dams still encounter difficulties to correctly characterize the geotechnical processes associated to the episodes of sudden enlargement of the breach. The most common way of modeling these phe-

nomena is by introducing a critical angle that, when the local breach slope becomes larger, causes a sudden enlargement of the breach sides leaving a residual or bearing angle.

There is a pressing need to better describe the mass instabilization episodes during dam overtopping and to effectively implement these phenomena in a numerical tool. The description of sediment transport in the dam body is, currently, also not entirely validated. These shortcomings in existing modeling approaches motivated the present work.

3 Conceptual Model

3.1 Governing Equations

The system of equations is composed of total mass conservation, equation (1), total momentum conservation in the x and y directions, equations (2) and 3 respectively, and total conservation of the sediment mass presented in the domain, equation (4)

$$\partial_t h \; + \; \partial_x \left(hu\right) \; + \; \partial_y \left(hv\right) \quad = \quad -\partial_t Z_b \quad (1)$$

$$\partial_t \left(uh\right) + \partial_x \left(u^2 h + \tfrac{1}{2} g h^2\right) + \partial_y \left(uvh\right) = -gh\partial_x Z_b - \frac{1}{\rho_m}\partial_x hT_{xx} - \frac{1}{\rho_m}\partial_y hT_{xy} - \frac{\tau_{b,x}}{\rho_m} \quad (2)$$

$$\partial_t \left(vh\right) + \partial_x \left(vuh\right) + \partial_y \left(v^2 h + \tfrac{1}{2} g h^2\right) = -gh\partial_y Z_b - \frac{1}{\rho_m}\partial_x hT_{yx} - \frac{1}{\rho_m}\partial_y hT_{yy} - \frac{\tau_{b,y}}{\rho_m} \quad (3)$$

$$\partial_t \left(C_m h\right) + \partial_x \left(C_m hu\right) + \partial_y \left(C_m hv\right) = -(1-p)\partial_t Z_b + \frac{1}{A}\partial_t \partial V \quad (4)$$

where x, y are the space coordinates, t is time, h is the depth, u and v are the depth-averaged velocities in the x and y directions, respectively, Z_b is the bed elevation, ρ_m and C_m represent the depth-averaged density and concentration of the mixture, respectively, T_{ij} are the depth-averaged turbulent stresses and τ_b represents the friction exerted by the bed on the fluid. The bed variation $\partial_t Z_b$ in given by $(1-p)\partial_t Z_b = (q_s - q_s^*)/\Lambda$ where q_s is the sediment discharge, q_s^* is its capacity value and Λ is an adaptation length.It is noted that system (1) to (4) does not include dispersive terms.

4 Evolution of bed morphology

The structure of the flow is idealized as layered domain, and sediment transport happens in the contact layer. Ferreira (2005) proposed that the thickness of the contact load layer is related to the flux of kinetic energy associated to the fluctuating motion of moving grains due to local imbalance and global equilibrium of rates of production and dissipation of fluctuating kinetic energy, i.e. the more energy is generated at the bottom of the contact load layer, the larger the thickness to allow for complete dissipation.

The interaction between the contact load layer and the bottom generate frictional stresses and collisional stresses due to sediment particle collision. If the frictional stresses and collisional stresses across the frictional sublayer are not in equilibrium, then the bed will be vertically displaced (Canelas, 2010).

The sediment discharge q_s is given by:

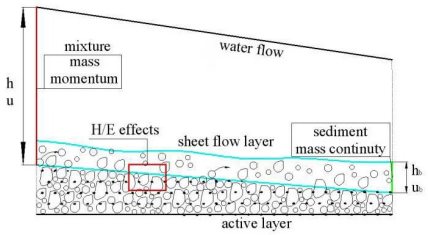

Figure 1: Layered flow structure composed by the bed or bottom, the transport or contact layer and the clear water layer. (Source: (Guan et al., 2014))

$$q_s = C_m \mathbf{u} h \tag{5}$$

where C_m is the depth averaged sediment concentration, $\mathbf{u}$ is the flow velocity and h is the depth of fluid.

The equilibrium sediment discharge is:

$$q_s = C_c^* \mathbf{u_c} h_c \tag{6}$$

where C_c^* is the layer-averaged capacity concentration in the contact load layer, u_c is the contact layer depth-averaged velocity and finally h_c is the thickness of the contact layer. The closure equation for h_c is given by:

$$\frac{h_c}{d_s} = m_1 + m_2 \theta \tag{7}$$

5 Discretization Scheme

The system of conservation equations presented in equations (1), (2), (3) coupled with the Exner equation for sediment transport, can be writen in form:

$$\begin{aligned} &\partial_t \boldsymbol{U}(\boldsymbol{V}) + \nabla \cdot \boldsymbol{E}(\boldsymbol{U}) = \boldsymbol{H}(\boldsymbol{U}) \Leftrightarrow \\ &\partial_t \boldsymbol{U}(\boldsymbol{V}) + \partial_x \boldsymbol{F}(\boldsymbol{U}) + \partial_y \boldsymbol{G}(\boldsymbol{U}) = \boldsymbol{H}(\boldsymbol{U}) \end{aligned} \tag{8}$$

Where V is the vector of primitive variables, H is the vector of conservative variables, F is the flux in the vector in the x direction, G is the flux in the vector in the y direction and H is the vector of source terms, the later of which can be subdived as $H = R + T + S$, where R expresses the friction and vertical fluxes, T represents the bottom source terms and S relates to the stratification and variation of density.

The dependent non-conservative variables variables in V, conservative variables in H and fluxes in F and G are:

$$\begin{aligned} \boldsymbol{V} &= \begin{bmatrix} h \\ u \\ v \\ C_m \end{bmatrix}; \quad \boldsymbol{U} = \begin{bmatrix} h \\ uh \\ vh \\ C_m h \end{bmatrix}; \\ \boldsymbol{F} &= \begin{bmatrix} uh \\ u^2 h + \frac{1}{2} g h^2 \\ uvh \\ C_m hu \end{bmatrix}; \quad \boldsymbol{G} = \begin{bmatrix} vh \\ vuh \\ v^2 h + \frac{1}{2} g h^2 \\ C_m hv \end{bmatrix} \end{aligned} \tag{9}$$

and the source terms in R and T are:

$$\boldsymbol{R} = \begin{bmatrix} -\partial_t Z_b \\ -\frac{\tau_{b,x}}{\rho^{(w)}} \\ -\frac{\tau_{b,y}}{\rho^{(w)}} \\ -(1-p)\partial_t Z_b \end{bmatrix}; \quad \boldsymbol{T} = \begin{bmatrix} 0 \\ -gh\partial_x Z_b \\ -gh\partial_y Z_b \\ 0 \end{bmatrix}. \tag{10}$$

Assuming the representation is piecewise, and that the cell area is A_i , and performing the boundary integral on the n_i edges of the cell i, one obtains:

$$\partial_t A_i \langle \boldsymbol{U}_i \rangle + \sum_{k=1}^{N} L_k \langle \boldsymbol{E} \cdot n \rangle_{ik} = A_i \langle \boldsymbol{H}_i \rangle \quad (11)$$

where $\langle\rangle$ represents the spatial average in the cell and L_k is the length of the k edge.

The flux variations can be expressed as a function of the conservative variables using an approximate Jacobian matrix, orthogonal to the edge in question and are susceptible to be represented in a eigenvector based homogeneous system.

The approximate variables are u, v,c (velocity of small perturbations) and C_m are:

$$\tilde{u}_{ik} = \frac{u_i\sqrt{h_i} + u_j\sqrt{h_j}}{\sqrt{h_i} + \sqrt{h_j}}; \quad \tilde{v}_{ik} = \frac{v_i\sqrt{h_i} + v_j\sqrt{h_j}}{\sqrt{h_i} + \sqrt{h_j}};$$
$$\tilde{c}_{ik} = \sqrt{g\frac{h_i + h_j}{2}}; \quad \tilde{C}_{m_{ik}} = \frac{C_{m_i}\sqrt{h_i} + C_{m_j}\sqrt{h_j}}{\sqrt{h_i} + \sqrt{h_j}} \quad (12)$$

With the average variables, the corresponding eigenvalues and eigenvectors are the calculated and given by:

$$\tilde{\lambda}^{(1)}_{ik} = (\tilde{\boldsymbol{u}} \cdot \boldsymbol{n} - \tilde{c})_{ik}; \quad \tilde{\lambda}^{(2)}_{ik} = (\tilde{\boldsymbol{u}} \cdot \boldsymbol{n})_{ik}; \quad (13)$$
$$\tilde{\lambda}^{(3)}_{ik} = (\tilde{\boldsymbol{u}} \cdot \boldsymbol{n} + \tilde{c})_{ik}; \quad \tilde{\lambda}^{(4)}_{ik} = (\tilde{\boldsymbol{u}} \cdot \boldsymbol{n})_{ik} \quad (14)$$

$$\tilde{\boldsymbol{e}}^{(1)}_{ik} = \begin{bmatrix} 1 \\ \tilde{u} - \tilde{c}n_x \\ \tilde{v} - \tilde{c}n_y \\ \tilde{C_m} \end{bmatrix}_{ik}; \quad \tilde{\boldsymbol{e}}^{(2)}_{ik} = \begin{bmatrix} 0 \\ -\tilde{c}n_y \\ \tilde{c}n_x \\ 0 \end{bmatrix}_{ik}; \quad (15)$$

$$\tilde{\boldsymbol{e}}^{(3)}_{ik} = \begin{bmatrix} 1 \\ \tilde{u} + \tilde{c}n_x \\ \tilde{v} + \tilde{c}n_y \\ \tilde{C_m} \end{bmatrix}_{ik}; \quad \tilde{\boldsymbol{e}}^{(4)}_{ik} = \begin{bmatrix} 0 \\ 0 \\ 0 \\ 1 \end{bmatrix}_{ik} \quad (16)$$

The Finite Volume Method discretization is then completed, with $N = 4$ as the eigenspace and considering a an orthogonal quadricular matrix with equally spaced squares, $k = 4$,

$$\boldsymbol{U}_i^{n+1} = \boldsymbol{U}_i^n - \frac{\Delta t}{A_i} \sum_{k=1}^{3} L_k$$
$$\sum_{n=1}^{4} \left(\tilde{\lambda}^{(n)}\alpha^{(n)} - \beta^{(n)}\right)^{-}_{ik} \tilde{\boldsymbol{e}}^{(n)}_{ik} + \Delta_t \left(T_i^{n+1}\right) \quad (17)$$

6 Results

6.1 Comparison between analytical solutions and numerical simulations

Dam-break test cases

Dam break test cases can be identified as an instantaneous removal of a barrier that initially separates 2 different constant states. If this description is valid, then the problem is a Riemann problem and admits self-similar solutions if the system of governing hyperbolic equations is homogeneous Ferreira (2005).

The numerical and analytical solutions of dam break test cases are discussed and presented, the first 2 are dam breaks in flat frictionless bottom, without sediment transport and with 2 different water heights on the right side. Considering $alpha = h_L/h_R$ for these test cases, that for the first two $\alpha = 0.1$ and $\alpha = 0.0$ respectively, the results for the analytical and numerical solution are presented in figures

For the Dambreak problem with sediment transport,$alpha = 0$ and no friction was regarded in the update of the velocity variables. Sediment discharge laws where of the same type

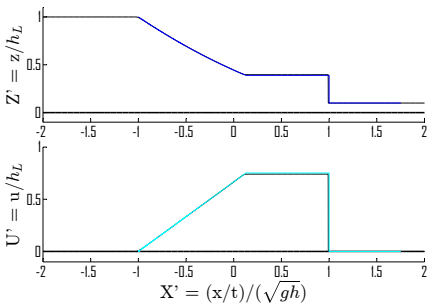

Figure 2: Comparison between analytical and numerical solution of the Stoker problem.(▬) Bottom elevation;(—) water elevation;(—) h - exact solution;(—) flow velocity;(—) u - exact solution

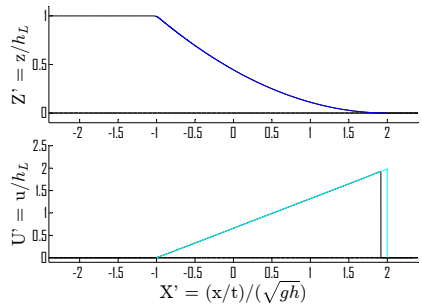

Figure 3: Comparison between analytical and numerical solution of the Ritter problem. (▬) Bottom elevation;(—) water elevation;(—) h - exact solution;(—) flow velocity;(—) u - exact solution

for both in that both feature a sediment discharge depending on the cube of the mean, depth-averaged, flow velocity Ferreira (2005).a quasi-equilibrium state of bottom rheology was considered.

Solution	h_L [m]	h_R [m]	Y_{bL} [m]	Y_{bR} [m]	a_c	d_s[m]	s
Type A	0.40	0.00	0.00	0.00	0.0010142	0.003	1.5
	0.40	0.00	0.00	0.10	0.0010142	0.003	1.5
Type B	0.40	0.10	0.08	0.00	0.0010142	0.003	1.5
	0.40	0.10	0.00	0.08	0.0010142	0.003	1.5

Table 1: Initial conditions for the 2 types of solution for the geomorphic dam break problem

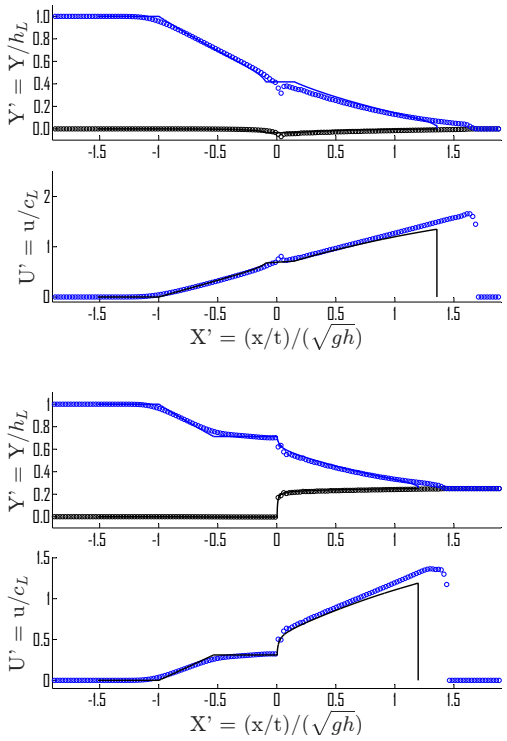

Figure 4: Numerical simulation of Type A solution for 2 different initial conditions. (▬) Bottom elevation - analytical solution;(o o o) Bottom elevation;(—) water elevation - analytical solution;(o o o) water elevation;(o o o) flow velocity;(—) flow velocity - analytical solution

2D test cases

2D test cases where performed in order to evaluate the simulate the analytical solutions to the water movement in parabolic basins, derived by (Thacker, 1981). The Initial conditions are shown in figures 6 for $t_0 = T/8$ and 7 for $t = 0s$

The results show good agreement between numerical and analytical solutions.

Simulation of dam breach and comparison with experimental work

Experimental work performed at LNEC was conducted to model the dam breaching process in small scale dams with good geotechni-

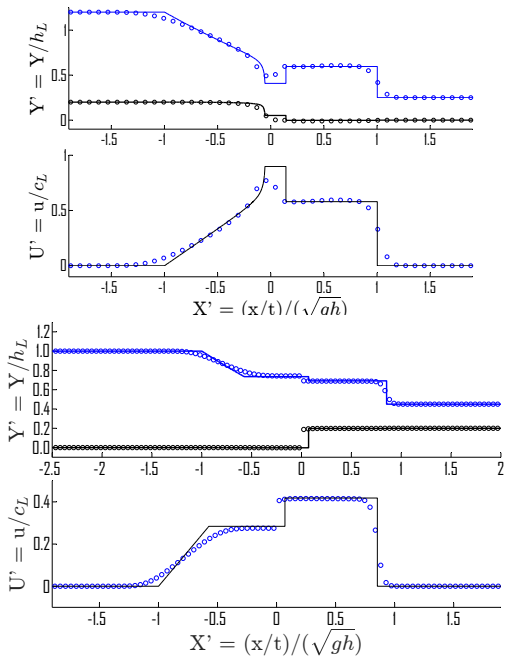

Figure 5: Numerical simulation of Type A solution for 2 different initial conditions. (━) Bottom elevation - analytical solution;(o o o) Bottom elevation;(—) water elevation - analytical solution;(o o o) water elevation;(o o o) flow velocity;(—) flow velocity - analytical solution

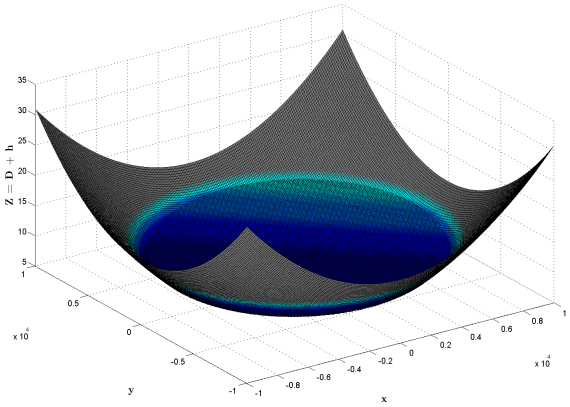

Figure 6: Initial profile for planar oscillation problem

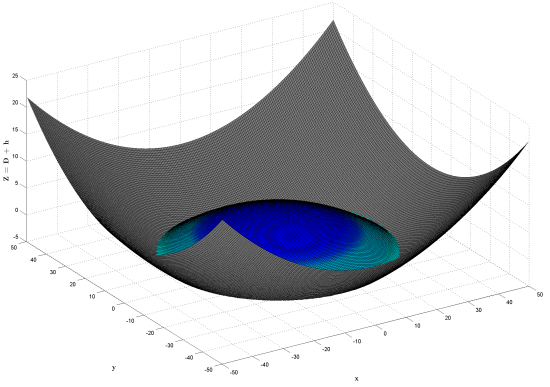

Figure 7: Initial profile for curved oscillation problem

cal design requirements. The results obtained provided both direct and indirect estimations of the breach hydrographs as a documented breaching process. The model is used to simulate the breaching of an embankment similar do the ones experimented. The geometries of the two embankments compared are presented in figures:

The domain is composed of 10×10 cm cells. The water that flow trough the breach is collected at a reservoir downstream, and the water is put back in the domain, upstream of the breaching zone, distributed over an are, as to not disturb the area near the breach.

The final breaching hydrograph is then obtained and compared with the one from trial 2, and the comparison is presented in figure 11:

The peak discharge is able to be reached for the numerical model, and the evolution of the discharge is similar do the experimental results, showing a good agreement between numerical and experimental work, for very similar embankment characteristics. Note that the hydrograph evolution is smoother, because the instabilization engine does not consider sudden breach enlargements, and thus it takes longer to reach the peak. This confirms the need for further work and development of a geotechnical instabilization algorithm that can reproduce the sliding of mass due to undercutting.

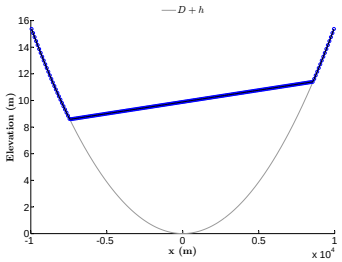

t = T/8

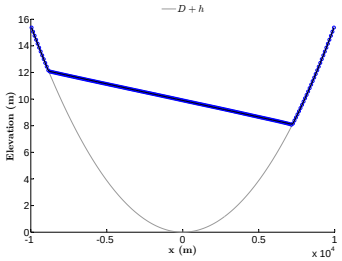

t = T/2

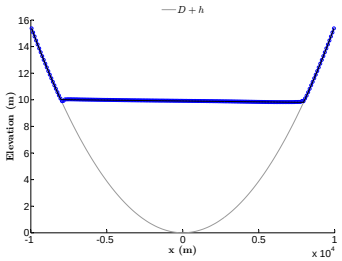

t = 3T/4

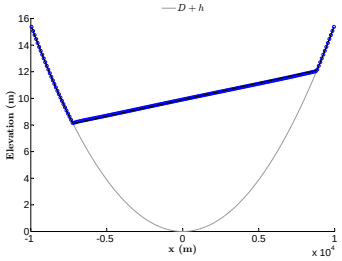

t = T

Figure 8: Water surface elevation in different instants, comparisson with analytical solution

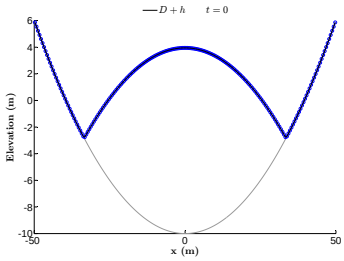

a)t = 0

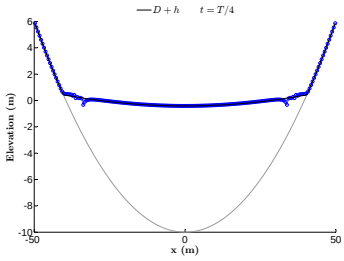

b)t = T/4

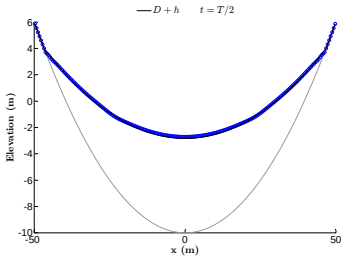

c)t = T/2

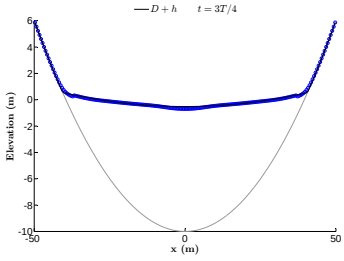

d)t = 3T/4

Figure 9: Water surface elevation in different instants, comparison with analytical solution

The bottom elevations for 2 time frames of the breaching process are presented in figures 12.

The bottom profiles are almost identical, and the shape is similar, although it is noticeable that more definition is needed in the proximity of the breach for a better characterization of the water elevation.

The water surface contours are presented for the same instant in figures 13 and 14

Similarities are evident on both water surface

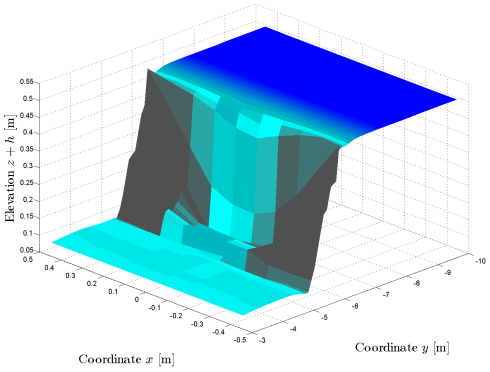

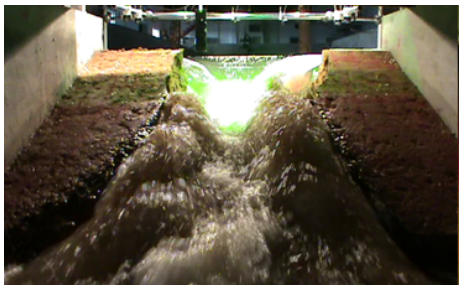

Figure 10: Initial geometry for embankment, model and experimental

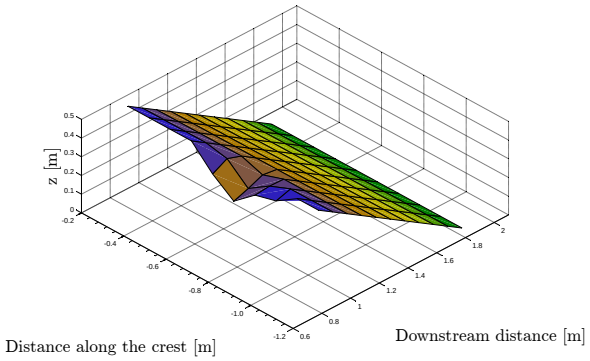

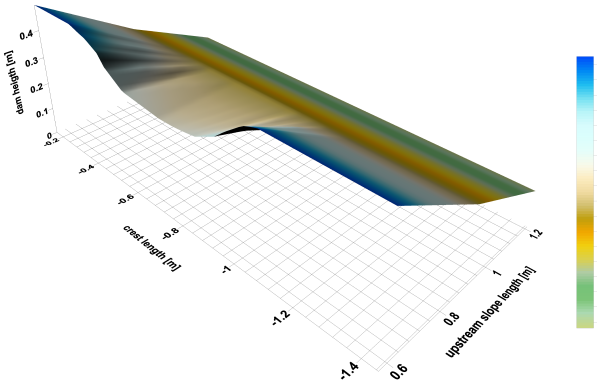

Figure 12: Upstream slope bottom geometry.Comparison with experimental data

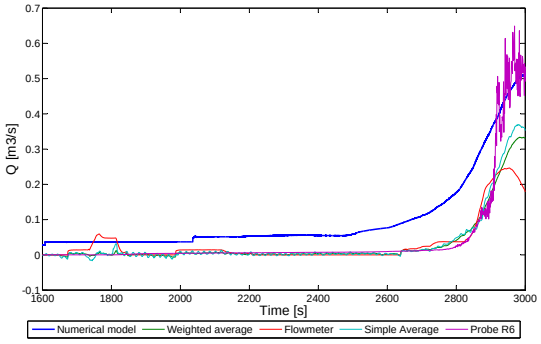

Figure 11: Comparison between numerical and experimental outflow hydrographs for trial 2

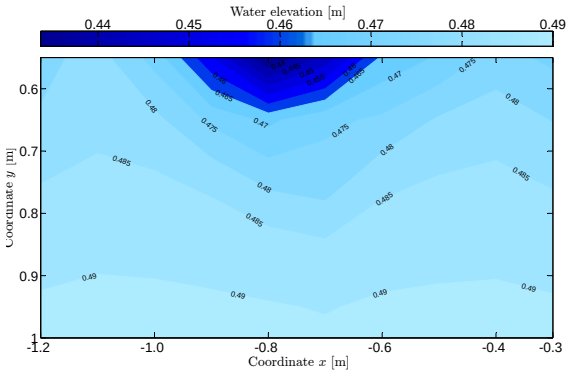

Figure 13: Water Surface contours for the simulation of experiment 2.

maps and the same definition problem is posed, but despite this the water elevation is in good agreement with the experimental data as the water profile contours follow a similar path.

7 Conclusions

In this work, an effort to simulate the breaching process of dams was undertaken. A numerical

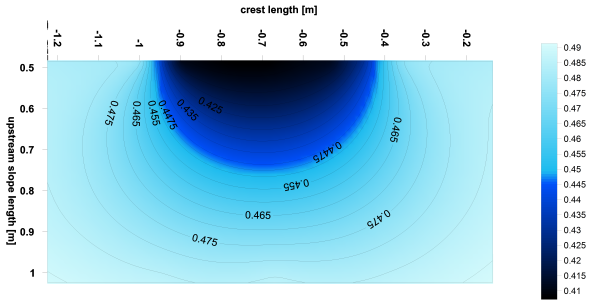

Figure 14: Water Surface contours for experiment 2.

model was developed using a simple high-level language, MATLAB, meant to become the core of a toolbox. It is envisaged that a dam-breach MATLAB toolbox would be subjected to a wide interest in the water resources community thus contributing to advance the confidence of users in deterministic tools to estimate breach hydrographs.

The conservation equations are essentially the shallow water equations complemented with mass conservation equations and a bed morphology equation. The model features non-equilibrium sediment transport. The closure equations were taken from existing literature on fluvial transport and sheet-flow (intense bed-load transport) studies. The discretization method, drawn from previous studies Canelas et al. (2013), is fully conservative, robust and obeys C-property.

The model, named STAVBreach, as a upgraded installment of the model used by Canelas et al. (2011), was validated with one-dimensional and two-dimensional solutions of the shallow water equations with and without sediment transport. The agreement between the simulations and the theoretical results was satisfactory. In particular, the conservation equations proved to be able to describe the water movement and the bed configuration for several well-known cases with analytical solutions.

However, some problems were detected, mostly in the numerical discretization approach. The problems proposed by Thacker for water movement in parabolic basins with flat and curved surfaces posed some difficulties on the simulations, due to the multiple wetting and drying fronts, as well as evident mesh rigidity observed. The Riemann problems consisting of geomorphic dam breaks with variations on the water level and bottom elevations revealed that the numerical scheme has trouble simulating the shock waves celerity and propagation as well as defining the constant state due to the non-equilibrium nature of the sediment transport equations used. The scheme was confirmed to be somewhat dissipative. Additionally some problems were in what concerns the rigidity imposed by the quadrangular mesh.

Experiments conducted at a medium-scale laboratory facility at LNEC provided data for a more complex validation phase. Outflow hydrographs, determined from two different methods, were obtained as well as data for characterization of the breaching process.

The instabilization conceptual model employed to describe the mass detachment phenomena observed at the banks of the pilot channel proved to be satisfactory but not ideal. The enlargement os the breach sides was correctly modeled but with artificial values of geotechnical parameters. It is clear that the instabilization phenomena needs to be described with more detail, namely with the inclusion of three-dimensional phenomena such as undercutting, in order to be able to simulate the sudden breach enlargements observed in the experiments.

References

Canelas, R. (2010). *2D Mathematical Modeling of Discontinuous Shallow Sediment-laden Flows*. Ph. D. thesis, Instituto Superior Técnico.

Canelas, R., J. Murillo, and R. Ferreira (2011). 2d simulation of discontinuous shallow flows. In *Experimental Methods in Hydraulic Research*, pp. 141–153. Springer.

Canelas, R., J. Murillo, and R. M. Ferreira (2013). Two-dimensional depth-averaged modelling of dam-break flows over mobile beds. *Journal of Hydraulic Research 51*(4), 392–407.

Ferreira, R. M. L. (2005). *River Morphodynamics and Sediment Transport - Conceptual Model and Solutions*. Ph. D. thesis, Instituto Superior Técnico.

Guan, M., N. G. Wright, and P. A. Sleigh (2014). 2d process-based morphodynamic model for flooding by noncohesive dyke breach. *Journal of Hydraulic Engineering 140*(7).

Thacker, W. C. (1981). Some exact solutions to the nonlinear shallow-water wave equations. *Journal of Fluid Mechanics 107*, 499 – 508.